SUPPLEMENTARY INFORMATION

A proteolytic AAA+ machine poised to unfold protein substrates

Alireza Ghanbarpour[1,2], Robert T. Sauer[2,*,✉], and Joseph H. Davis[2,*,✉]

[1]Department of Biochemistry and Molecular Biophysics
Washington University in St. Louis
St Louis, USA 63130

[2]Department of Biology
Massachusetts Institute of Technology
Cambridge, USA 02139

*Equal contributions

✉ Correspondence: bobsauer@mit.edu, jhdavis@mit.edu

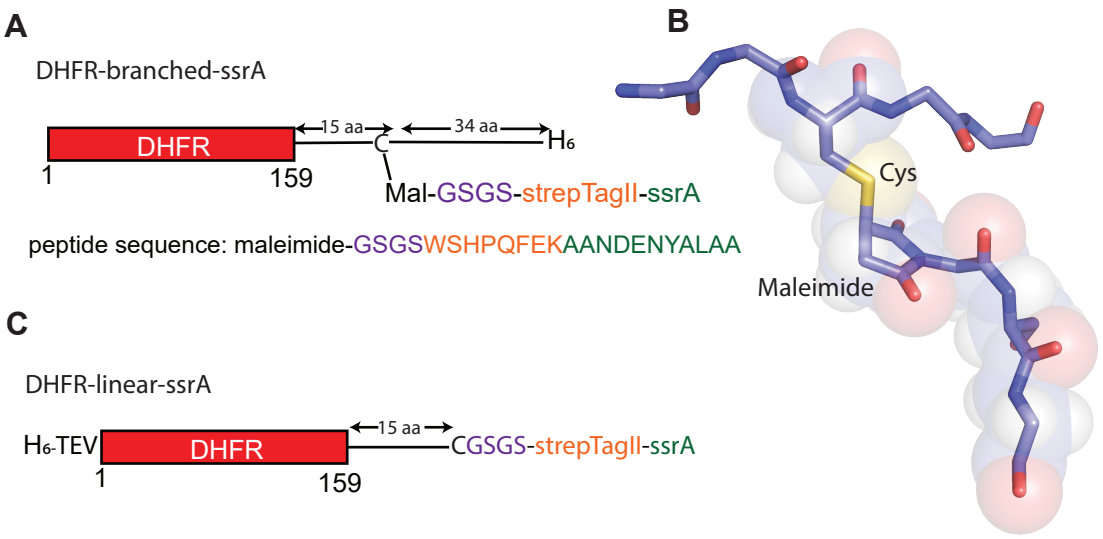

Supplemental Figure 1. Schematic and 3D representations of branched-degron **(A, B)** and linear-degron DHFR substrates **(C)**.

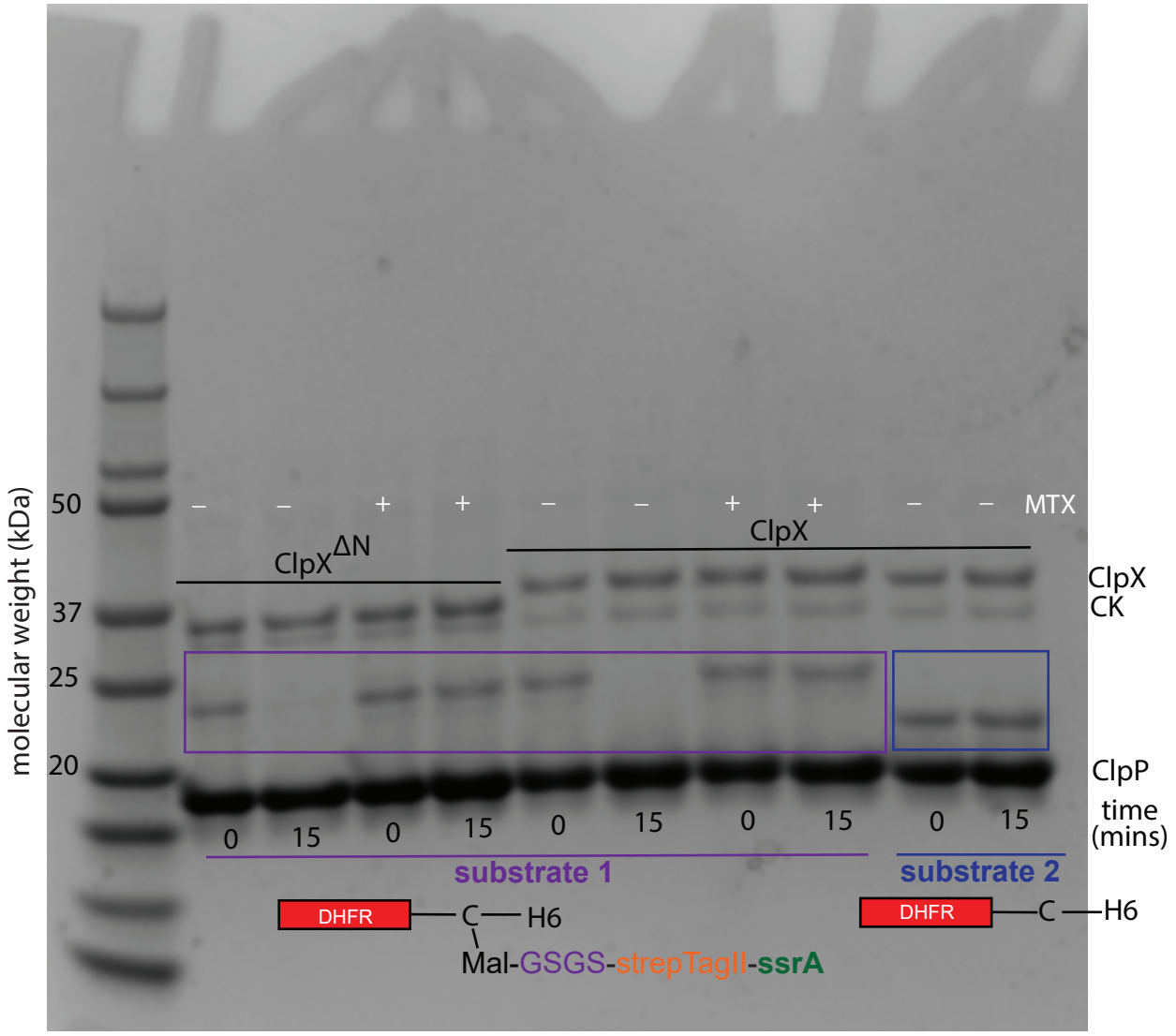

Supplemental Figure 2. Degradation of branched-degron DHFR (substrate 1, 5 μM) by $ClpX_6^{\Delta N}$ or full-length $ClpX_6$ (0.5 μM) and $ClpP_{14}$ (1.5 μM) was assayed by SDS-PAGE gel in the presence or absence of MTX (20 μM). No degradation of a DHFR substrate without the ssrA tag (substrate 2) was observed in the absence of MTX.

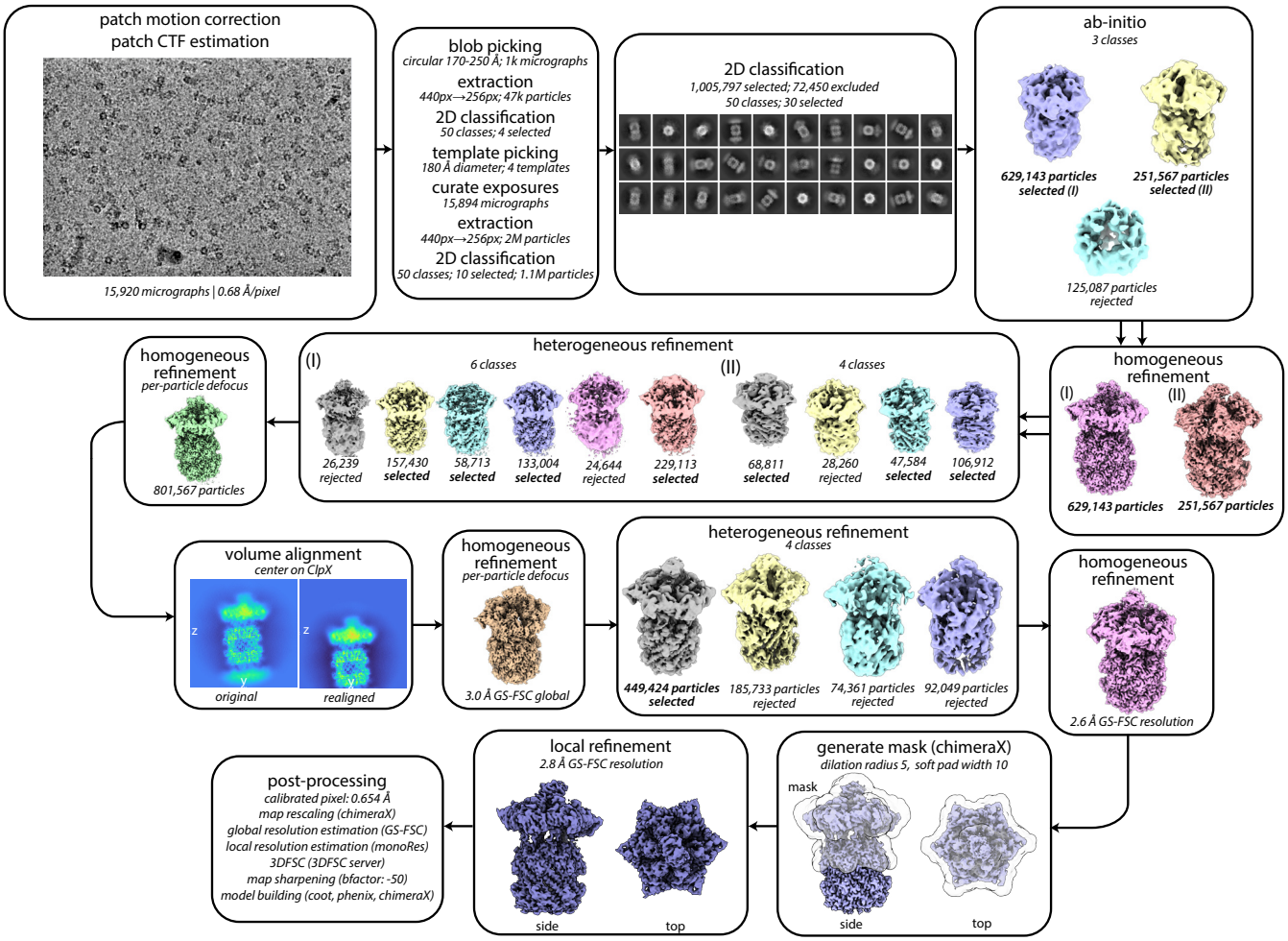

Supplementary Figure 3. Image processing workflow: branched-dergon DHFR•MTX.
CryoSPARC processing workflow for single-chain ClpX$^{\Delta N}$/ClpP/branched-degron DHFR•MTX particles. Job names, job details, and non-default parameters (italicized) are noted in each box.

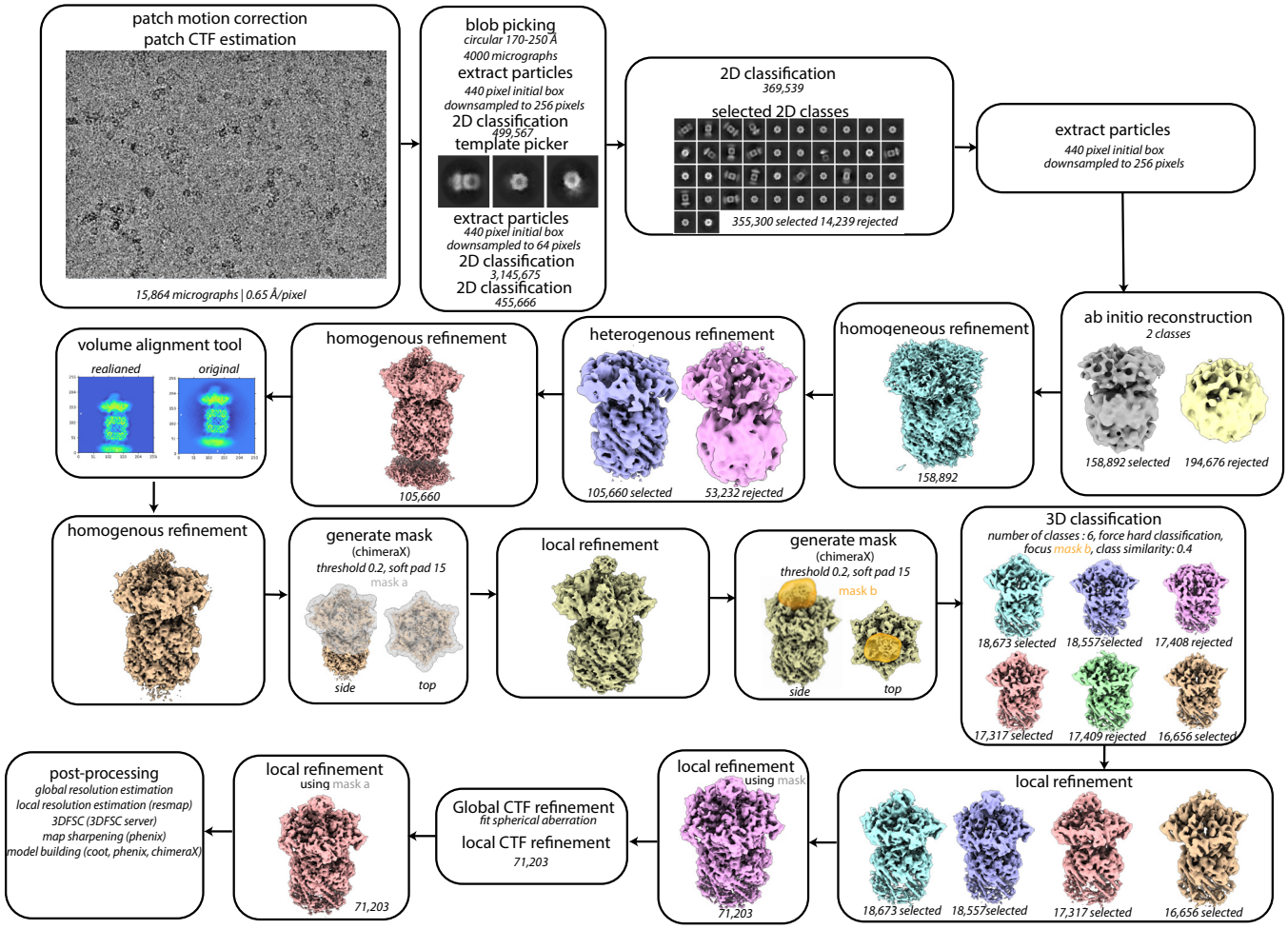

Supplementary Figure 4. Image processing workflow: linear-degron DHFR•MTX.
CryoSPARC processing workflow for single-chain ClpX$^{\Delta N}$/ClpP/linear-degron DHFR•MTX particles. Job names, job details, and non-default parameters (italicized) are noted in each box.

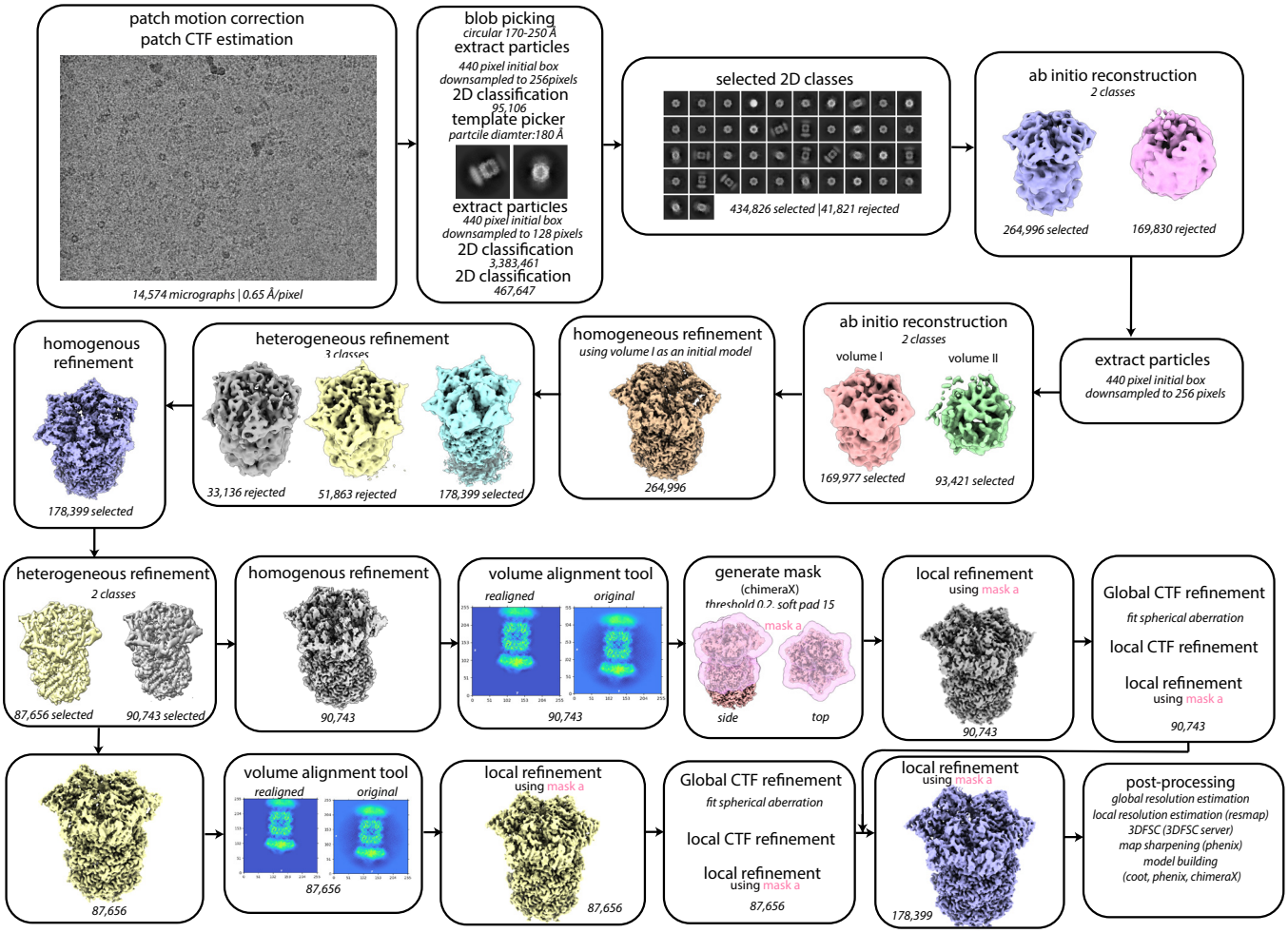

Supplementary Figure 5. Image processing workflow: branched-degron DHFR (no MTX).
CryoSPARC processing workflow for single-chain ClpX$^{\Delta N}$/ClpP/branched-degron DHFR (no MTX) particles. Job names, job details, and non-default parameters (italicized) are noted in each box.

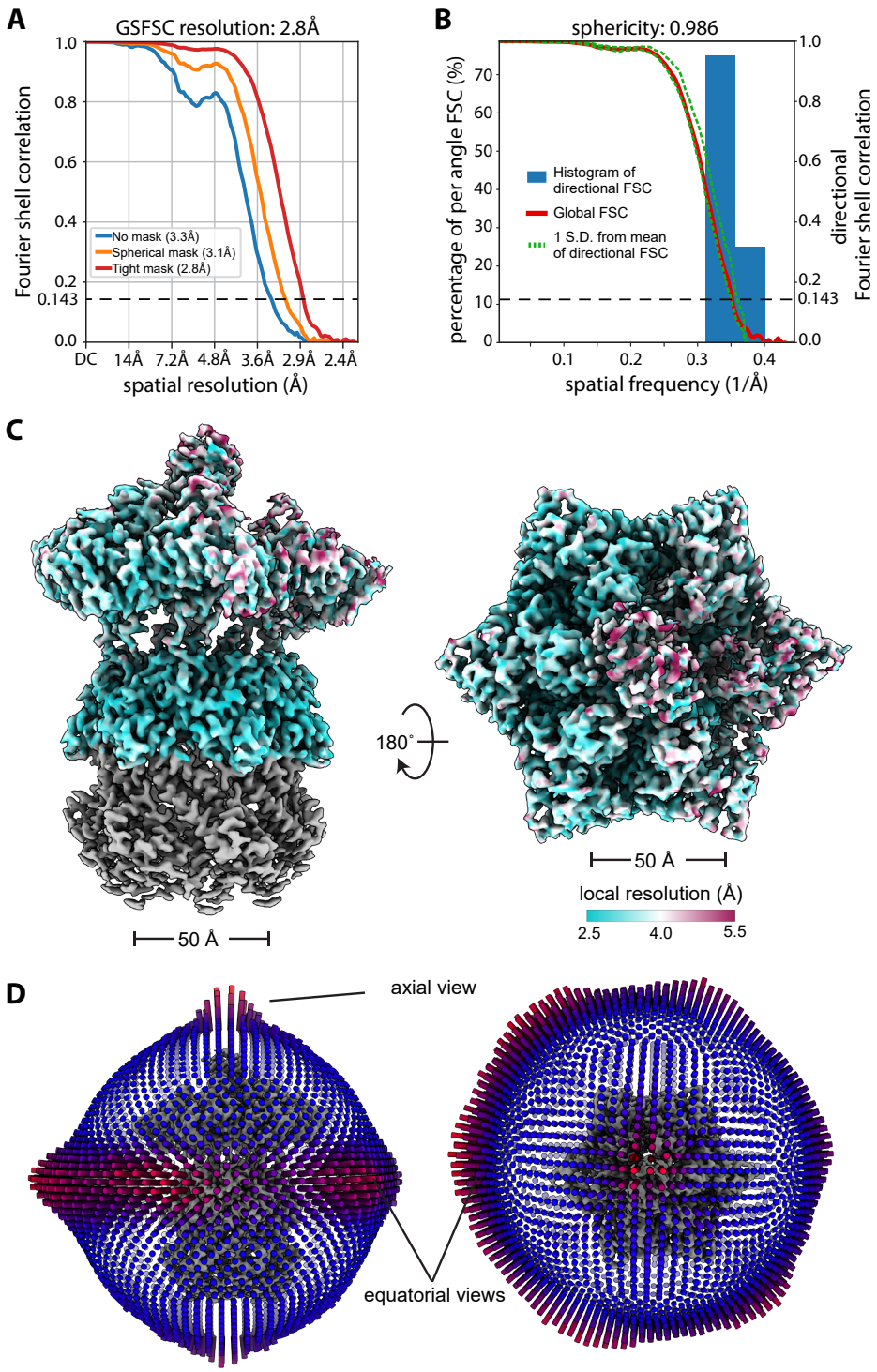

Supplementary Figure 6. Estimates of resolution and angular sampling: branched-degron DHFR•MTX.
(A) Global resolution estimated by the gold-standard Fourier Shell Correlation method as implemented in CryoSPARC (Punjani *et al.* 2017). **(B)** Directional FSC as estimated by the 3DFSC server (Tan *et al.* 2017). **(C)** Density map colored by local resolution as estimated by cryoSPARC's implementation of monoRes (Vilas *et al.* 2018). **(D)** Projection-angle distribution.

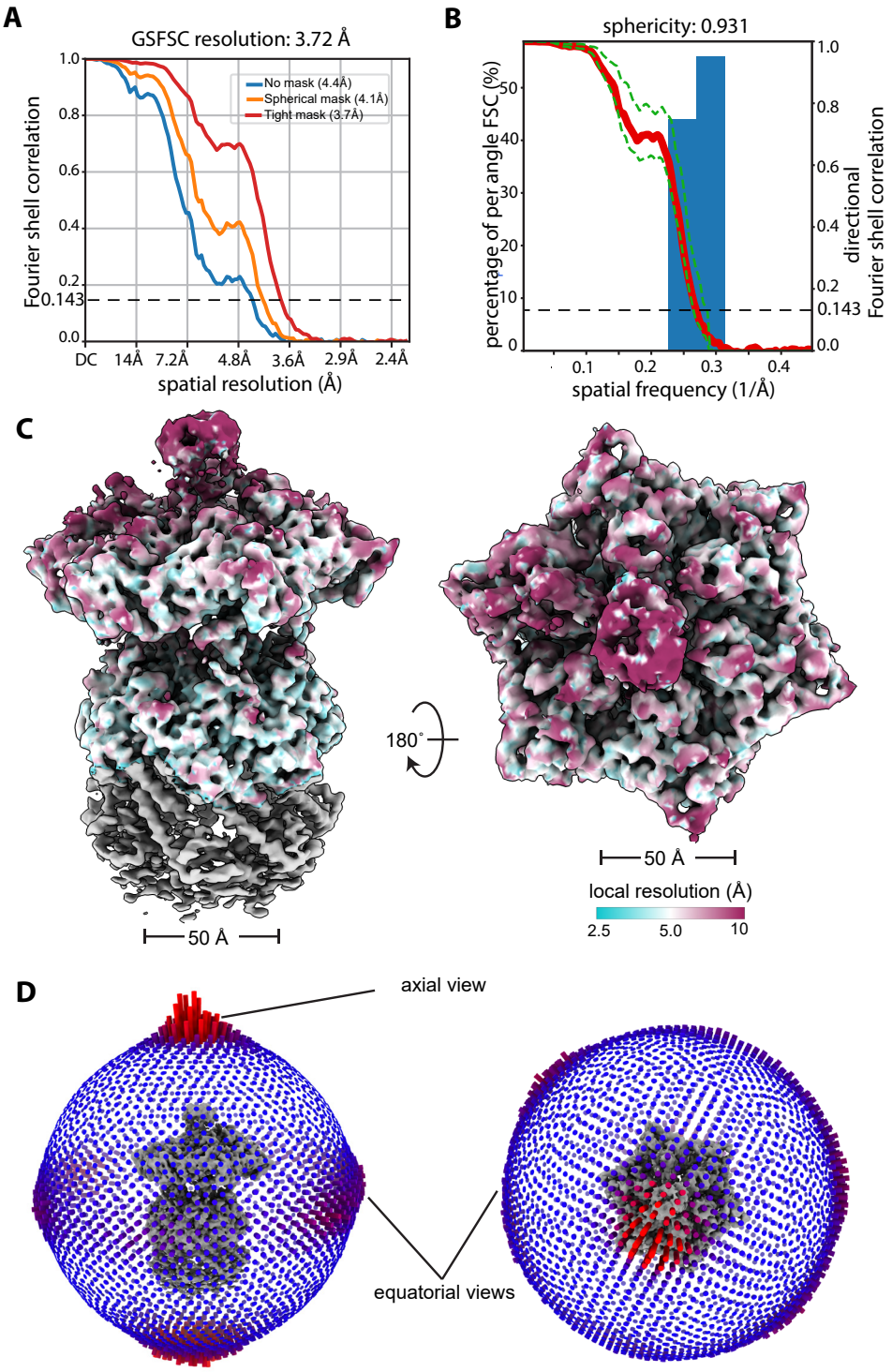

Supplementary Figure 7. Estimates of resolution and angular sampling: linear-degron DHFR•MTX.
(A) Global resolution estimated by the gold-standard Fourier Shell Correlation method as implemented in CryoSPARC (Punjani *et al.* 2017). **(B)** Directional FSC as estimated by the 3DFSC server (Tan *et al.* 2017). **(C)** Density map colored by local resolution as estimated by cryoSPARC's implementation of monoRes (Vilas *et al.* 2018). **(D)** Projection-angle distribution.

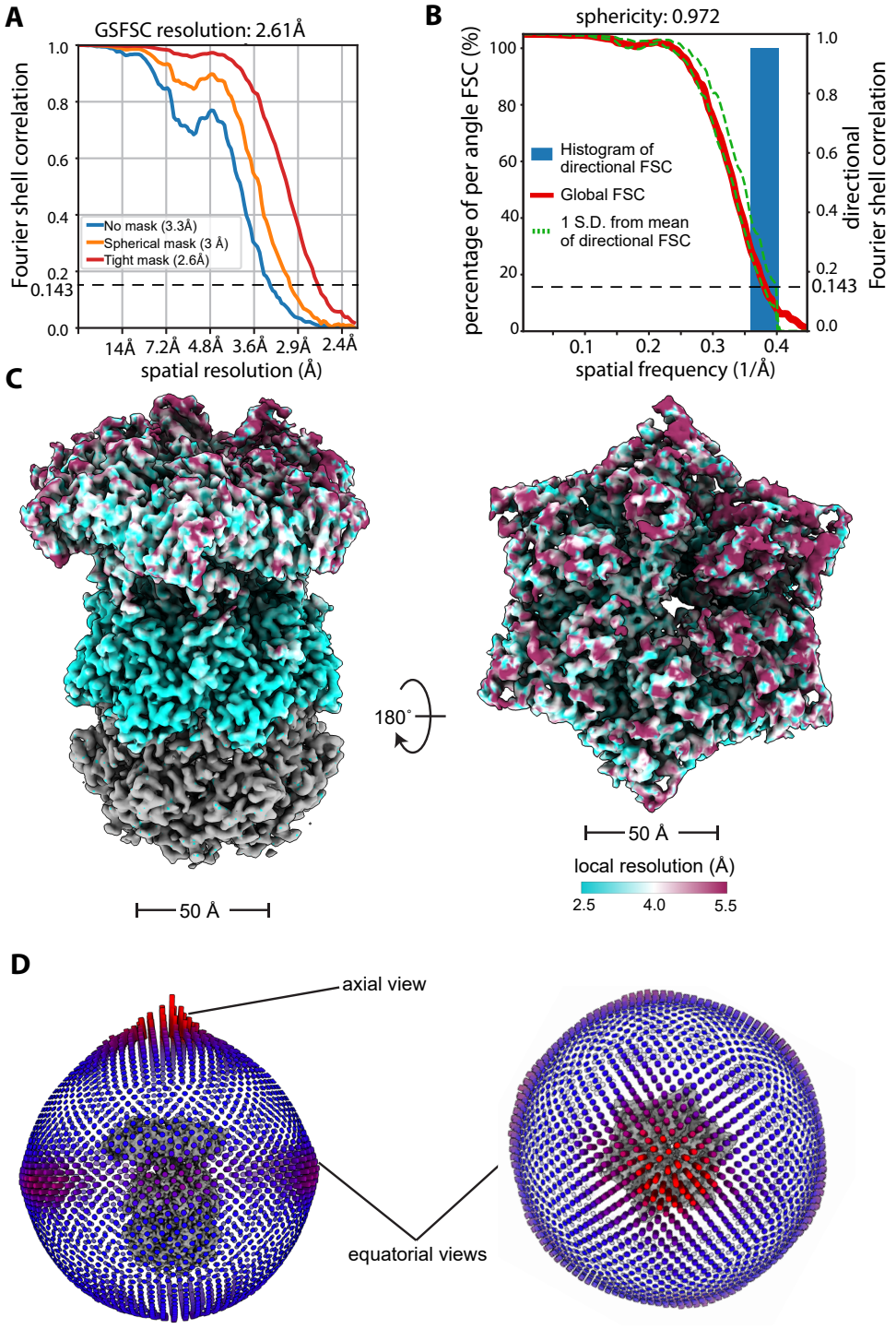

Supplementary Figure 8. Estimates of resolution and angular sampling: branched-degron DHFR (no MTX).
(A) Global resolution estimated by the gold-standard Fourier Shell Correlation method as implemented in CryoSPARC (Punjani *et al.* 2017). **(B)** Directional FSC as estimated by the 3DFSC server (Tan *et al.* 2017). **(C)** Density map colored by local resolution as estimated by cryoSPARC's implementation of monoRes (Vilas *et al.* 2018). **(D)** Projection-angle distribution.

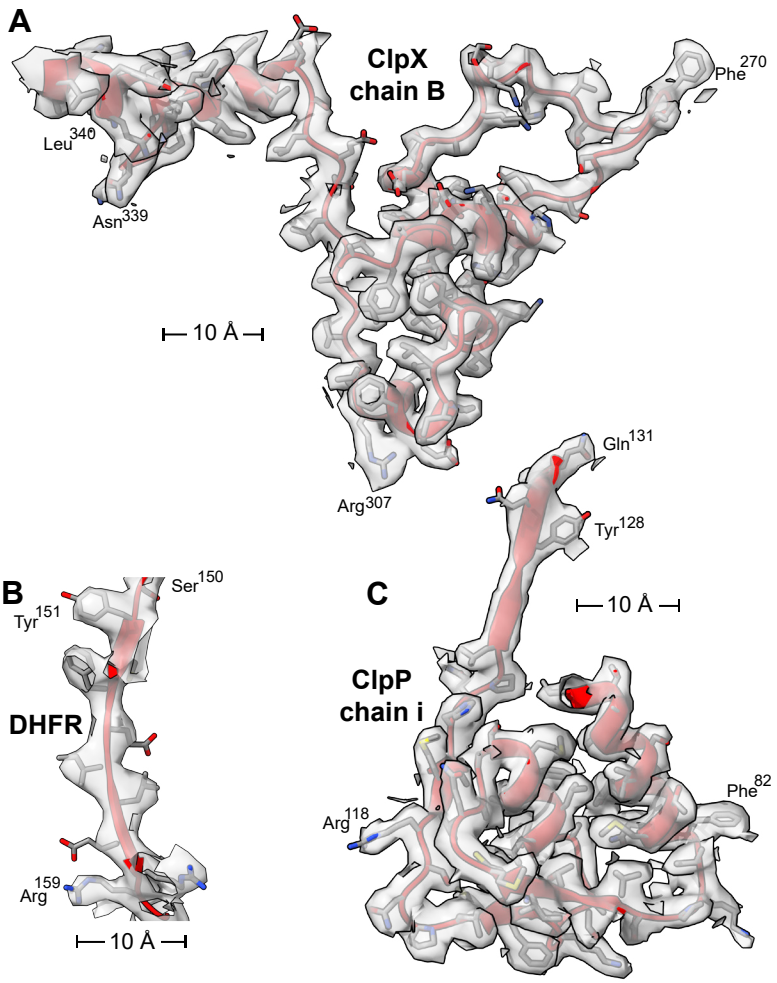

Supplementary Figure 9. Cryo-EM density map and atomic model: branched-degron DHFR•MTX.
Cryo-EM density map (grey semi-transparent surface) overlayed on the fitted atomic models, with secondary structure elements colored red, and side chains colored by atom type. **(A)** ClpX residues 270-340 of chain B[2]. **(B)** DHFR residues 150-160. **(C)** ClpP residues 82-131 of chain i.

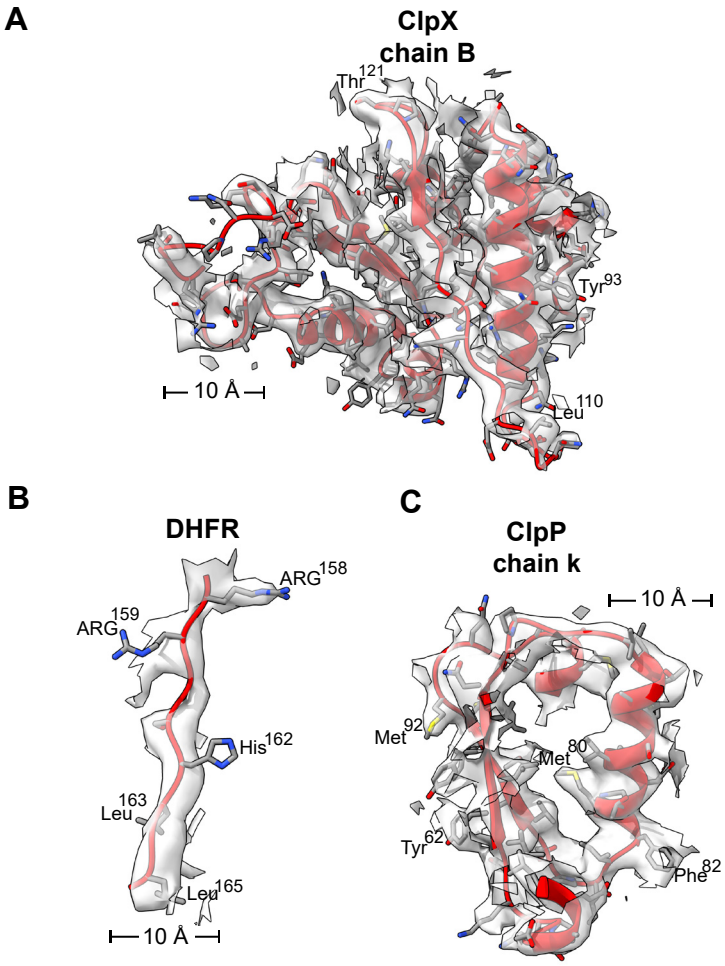

Supplementary Figure 10. Cryo-EM density map and atomic model: linear-degron DHFR•MTX.
Cryo-EM density map (grey semi-transparent surface) overlayed on the fitted atomic models, with secondary structure elements colored red, and side chains colored by atom type. **(A)** ClpX residues 50-200 of chain B[2]. **(B)** DHFR residues 158-165. **(C)** ClpP residues 50-100 of chain k.

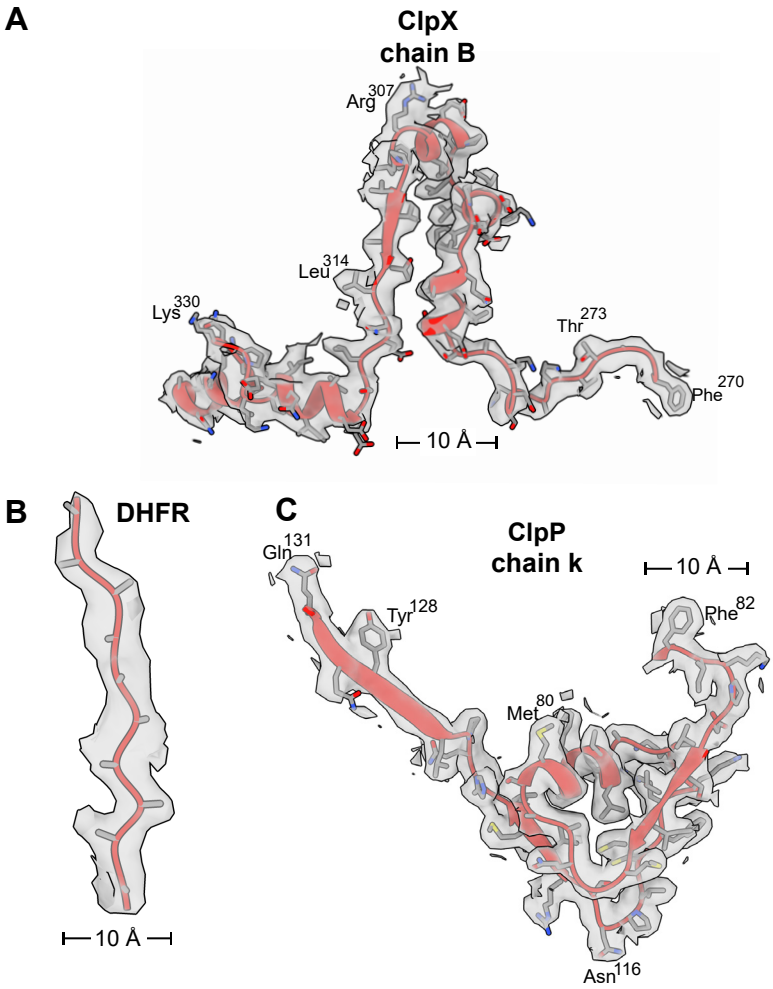

Supplementary Figure 11. Cryo-EM density map and atomic model: branched-degron DHFR (no MTX).
Cryo-EM density map (grey semi-transparent surface) overlayed on the fitted atomic models, with secondary structure elements colored red, and side chains colored by atom type. **(A)** ClpX residues 270-340 of chain B[2]. **(B)** DHFR residues 150-160. **(C)** ClpP residues 82-131 of chain i.

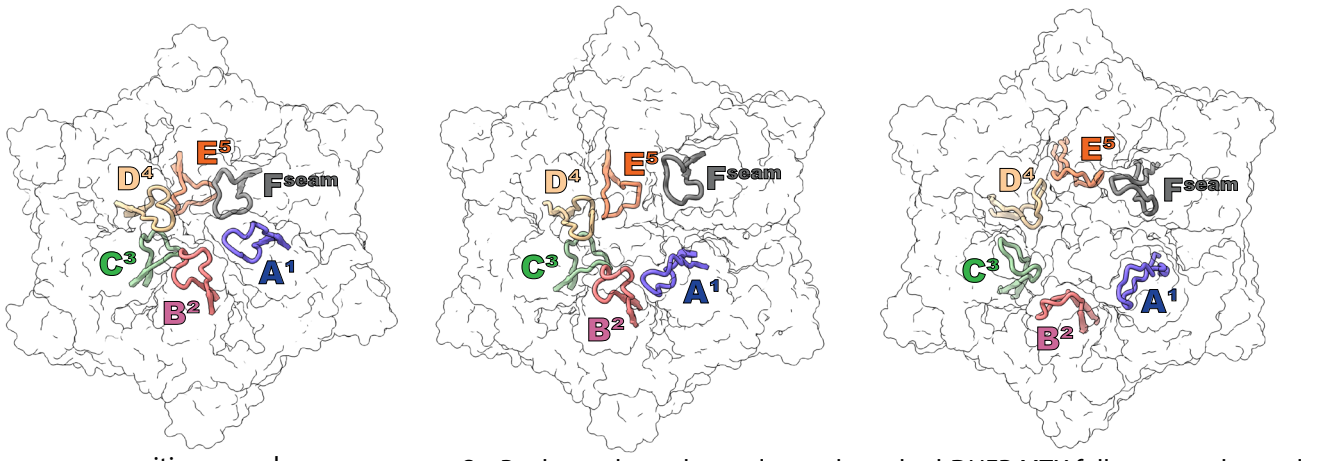

recognition complex
[6WRF]

SspB adapter-bound complex
[8ET3]

branched-DHFR·MTX fully engaged complex
[8V9R: this work]

Supplementary Figure 12. Conformational flexibility of ClpX RKH loops.
Diverse conformations of RKH loops (residues 218-240 shown in cartoon representation) from ClpXP structure 6WRF (left) (Fei *et al.* 2020), 8ET3 (center) (Ghanbarpour *et al.* 2023), and ClpXP bound to branched-degron DHFR•MTX (PDB code 8V9R) from this study (right). Subunit colors: A^1 (purple), B^2 (salmon), C^3 (green); D^4 (wheat), E^5 (orange), and F^{seam} (gray).

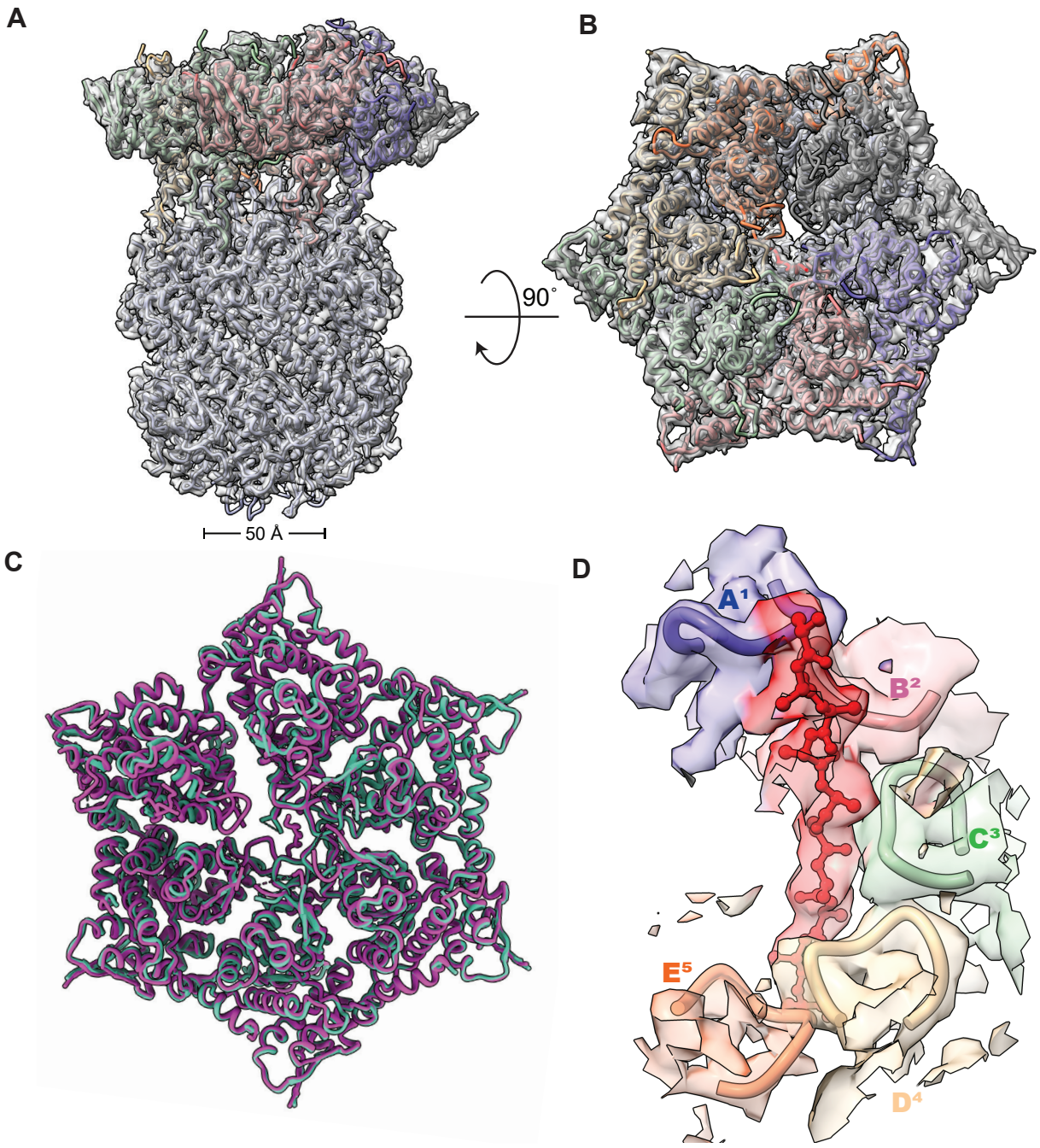

Supplementary Figure 13. Structure of ClpXP determined with branched-degron DHFR in the absence of MTX closely resembles the previous 6WSG translocation complex.

(A,B) Overlaid density maps and models for structure ClpX$^{\Delta N}$•ClpP•branched-DHFR (PDB ID: 9C88) are shown in side and top views, respectively. Note that substrate density above the axial channel is absent in panel A. **(C)** Cartoon overlay of ClpX structures from structure ClpX$^{\Delta N}$•ClpP•branched-DHFR (PDB code 9C88: purple) and the translocation complex (PDB code 6WSG: green). **(D)** Overlaid density map and atomic model for structure ClpX$^{\Delta N}$•ClpP•branched-DHFR shows that the pore-1 loops (residues 150-155) of ClpX chains A^1, B^2, C^3, D^4 and E^5 assume a spiral conformation that interacts with two-residue segments of the substrate polypeptide in a β-strand conformation (red ball and stick representation).

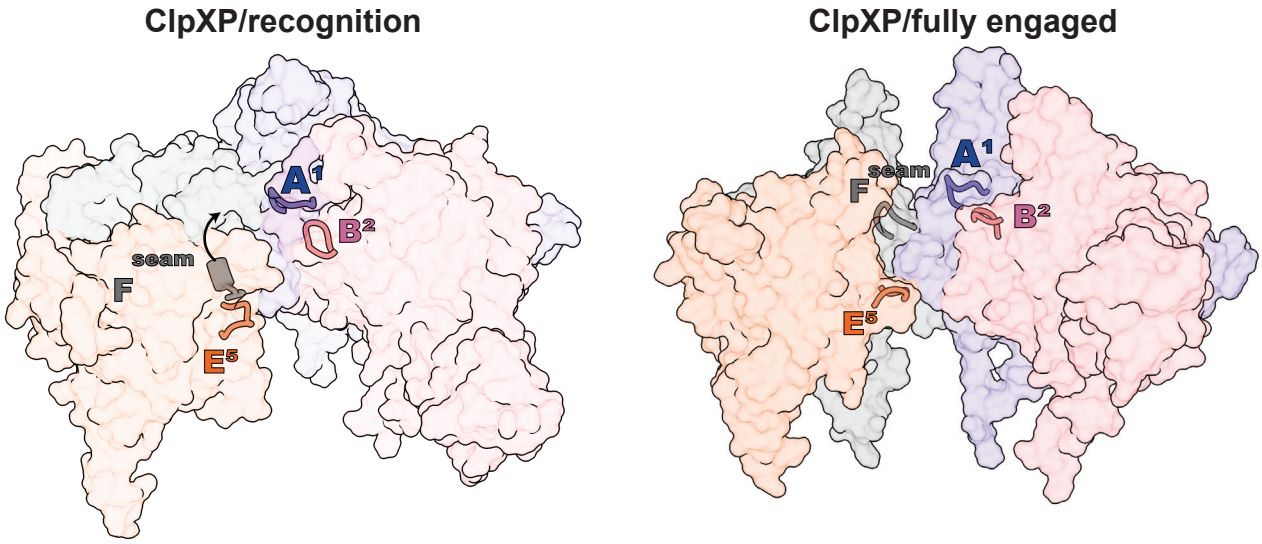

Supplementary Figure 14. The upward movement of F^{seam} pore-1 loop.
Comparison of the F^{seam} pore-1 loop location in the ClpXP recognition complex structure (PDB code 6WRF) at left, and ClpXP fully engaged complex at right (PDB code 8V9R: branched-degron-DHFR•MTX). The subunits C and D are hidden for clarity. The pore-1 loops (150-155) are shown in cartoon representation and are color-coded by subunits.

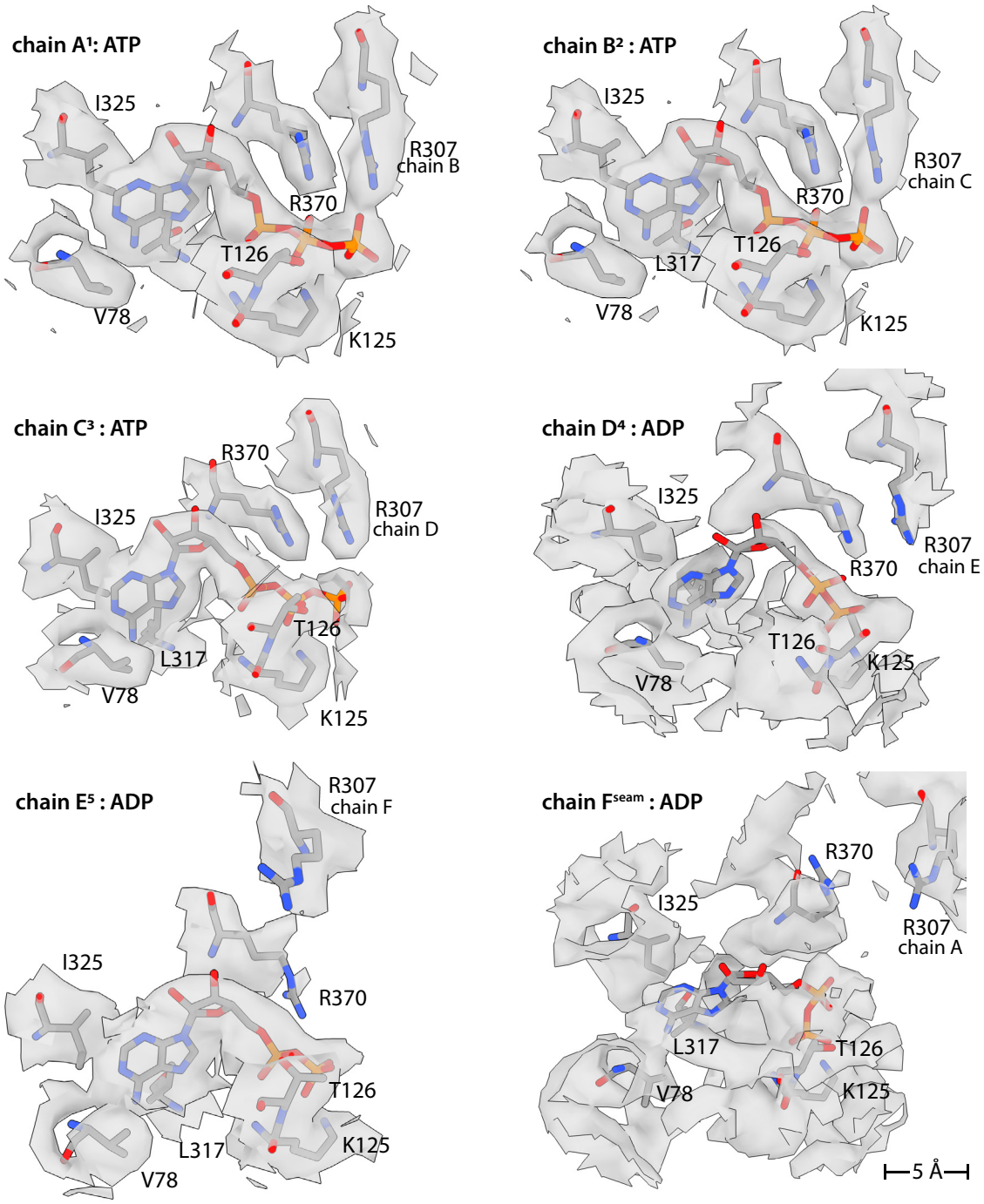

Supplementary Figure 15. Density for ATP or ADP bound to different ClpX subunits in the branched-DHFR•MTX fully engaged structure. Density map (grey semi-transparent surface) overlaid on atomic models colored by atom type.

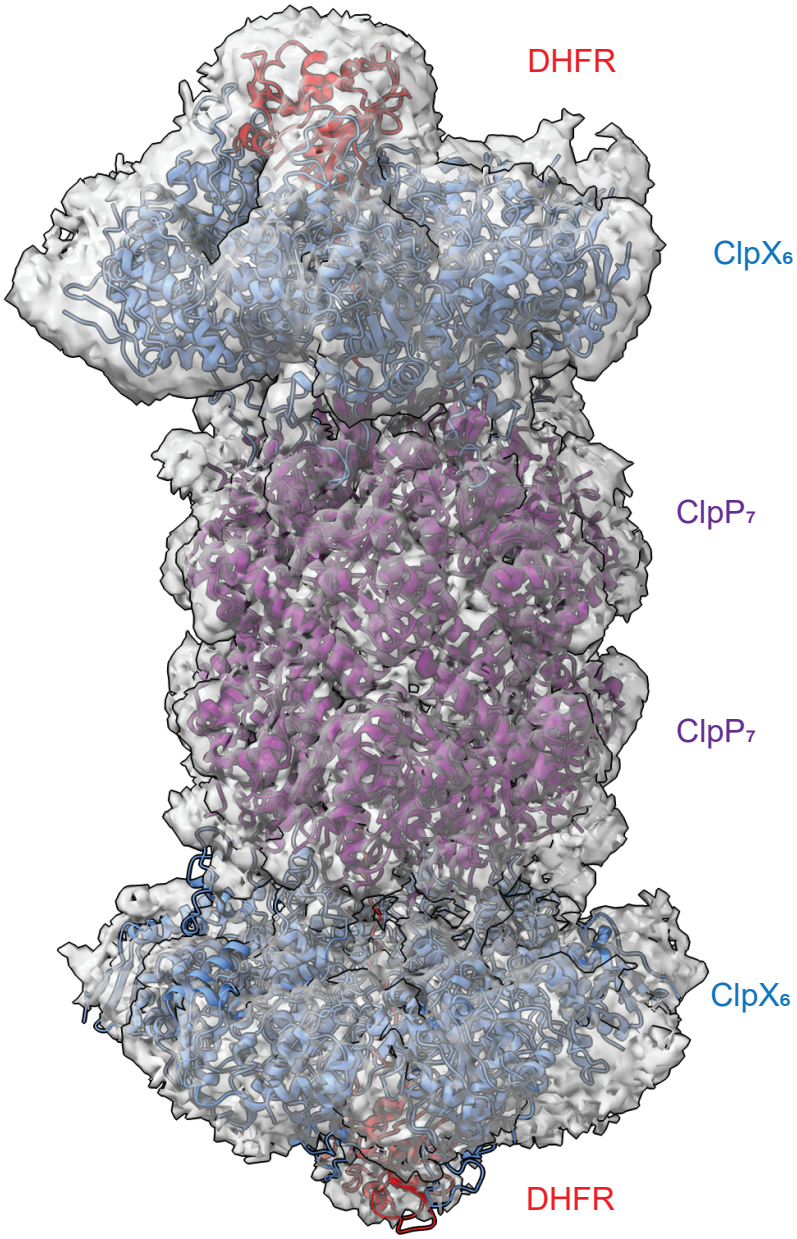

Supplementary Figure 16. Low-resolution structure of ClpX engaged with branched-degron DHFR•MTX bound to both heptameric rings of ClpP$_{14}$. The ClpX•DHFR complex on the bottom adopts multiple registers relative to the top complex and has low resolution as a consequence of conformational averaging.

Supplementary Movie 1. Movements of the F^{seam} subunit pore-1 loop. A morph between atomic models of the recognition complex (PDB code 6WRF) and the fully engaged branched-degron DHFR•MTX complex (PDB code 8V9R). In the morph, the pore-1 loop of the F^{seam} subunit in the substrate engaged structure has moved higher, positioning it closest to the pore-1 loop of subunit A^1 compared to its position in the recognition complex, where it is closest to the pore-1 loop of subunit E^5.

Supplementary Movie 2. Analysis of structural heterogeneity in the branched-degron DHFR•MTX complex. A sampling of 100 volumes sampled from the *k*-means cluster centroid locations of latent embeddings displayed over a fixed atomic model (PDB code 8V9R). Note that we did not observe structures with the F^{seam} subunit in the 'down' conformation or those with the subunit-E IGF loop in a different ClpP cleft.

Supplementary Movie 3. F^{seam} subunit conformations. A morph between the fully engaged (PDB code 8V9R) and ssrA tag recognition (PDB code 6WRF) conformations highlighting the motion in the F^{seam} subunit as it transitions from the 'up' to 'down' conformations. According to the 'large-step' model, such a motion could be used to pull substrate down through the axial pore.